AC-DC Security-Constrained Optimal Power Flow for the Australian National Electricity Market

Ghulam Mohy-ud-din[§], Rahmat Heidari[§], Hakan Ergun[†,‡], and Frederik Geth[*]
[§]Energy Systems, Energy, Commonwealth Scientific and Industrial Research Organisation (CSIRO), Newcastle, Australia
[†]Electa-ESAT, KU Leuven, Leuven, Belgium
[‡]Electrical Networks, EnergyVille, Genk, Belgium
[*]GridQube, Brisbane, Australia

***Abstract*—This paper presents a new methodology to solve the integrated ac-dc security-constrained optimal power flow (SCOPF) problem for large-scale power systems, with a focus on the Australian National Electricity Market (NEM). The proposed SCOPF is based on a decomposition scheme that significantly reduces the dimensionality of the problem and thus improves the computational performance. It further supports a contingency ranking, evaluation, and non-dominated filtering algorithm, cyclic selection of filtered contingencies, careful choice of slack variables, and a tailored warm start to the nonlinear problem. The methodology is validated against the two-stage mathematical programming model that uses an explicit nonlinear model of both the base case and the contingency cases, at a slightly higher cost but significantly faster execution. Moreover, the NEM power system, is studied addressing different scenarios including load variations, renewable energy zone integration, and additional reinforcements like point-to-point and meshed HVDC. The proposed approaches provides preventive solutions in less than 5 min thus affirming the model's effectiveness in real-time applications and planning studies.**

***Index Terms*—HVDC, converters, security-constrained optimal power flow, contingency filter, decomposition.**

NOMENCLATURE

Indices and sets

$c \in \mathcal{C}$	Set of converter stations
$d \in \mathcal{D}$	Set of dc branches
$e, f \in \mathcal{E}$	Set of dc nodes
$g \in \mathcal{G}$	Set of generators
$g \in \mathcal{G}_k$	Set of generators online in contingency k
$gi \in \mathcal{T}^{\text{g}}$	Tuple set of generators on bus i
$gi \in \mathcal{T}^{\text{g}}_k$	Tuple set of generators on bus i in contingency k
$i, j \in \mathcal{N}$	Set of ac nodes
$k \in \mathcal{K}$	Set of N-1 contingencies
$l \in \mathcal{L}$	Set of ac branches
$me \in \mathcal{T}^{\text{l,dc}}$	Tuple set of dc loads in bus i
$mi \in \mathcal{T}^{\text{l,ac}}$	Tuple set of ac loads in bus i
$r \in \mathcal{R}$	Set of reference nodes
$cei \in \mathcal{T}^{\text{cv,r}}$	Tuple set of converter station c from node $e \to i$
$cie \in \mathcal{T}^{\text{cv}}$	Tuple set of converter station c from node $i \to e$
$def \in \mathcal{T}^{\text{dc}}$	Tuple set of dc branch d from node $e \to f$
$dfe \in \mathcal{T}^{\text{dc,r}}$	Tuple set of dc branch d from node $f \to e$
$lij \in \mathcal{T}^{\text{ac}}$	Tuple set of ac branch l from node $i \to j$
$lji \in \mathcal{T}^{\text{ac,r}}$	Tuple set of ac branch l from node $j \to i$

Parameters

α_g	Participation factor of generator g
$\chi^{\text{dclodf}}_{ee(k)}$	dcLODF matrix entry $[e, e(k)]$
χ^{dcdf}_{ie}	DCDF matrix entry $[i, e]$
$\chi^{\text{lodf}}_{ii(k)}$	LODF matrix entry $[i, i(k)]$
χ^{ptdf}_{ij}	PTDF matrix entry $[i, j]$
χ^{lf}_{i}	Loss factor at node i
ψ	Penalty cost
ρ_d	Number of poles for dc branch d
$a^{\text{cv}}_c, b^{\text{cv}}_c, c^{\text{cv}}_c$	Converter loss coefficients for ac/dc converter c
b^{f}_c	Susceptance of converter station c filter
g_d	Conductance of dc branch d
P^{loss}	Total active power line losses
$P^{\text{out}}_{g,k}$	Active power outage in generator contingency k
P_m, Q_m	Active and reactive power load m
y^{pr}_c	Admittance of converter station c phase reactor
y^{tf}_c	Admittance of converter station c transformer
$y^{\text{sh,f}}_i$	Fixed shunt admittance at node i
$y^{\text{sh}}_{lij}, y^{\text{sh}}_{lji}$	Shunt admittances of ac branch l from node $i \rightleftarrows j$
y_l	Series admittance for ac branch l

Variables and bounds

$\overline{\delta\theta_{lij}}, \underline{\delta\theta_{lij}}$	Voltage angle difference in nodes $i \to j$ limits
φ_c	Firing angle of converter at station c, $\in [\underline{\varphi_c}, \overline{\varphi_c}]$
$\varsigma_{g,k}$	Slack variable for generator g power capacity violation in contingency k, $\in [\underline{\varsigma_g}, \overline{\varsigma_g}]$
$\varsigma_{l,k}$	Slack variable for ac branch l power flow violation in contingency k, $\in [\underline{\varsigma_{l,k}}, \overline{\varsigma_{l,k}}]$
$\lvert V^{\text{cv}}_c\rvert, \theta^{\text{cv}}_c$	Voltage at converter node in station c, $\in [\underline{V^{\text{cv}}_c}, \overline{V^{\text{cv}}_c}], [\underline{\theta^{\text{cv}}_c}, \overline{\theta^{\text{cv}}_c}]$
$\lvert V^{\text{f}}_c\rvert, \theta^{\text{f}}_c$	Voltage at filter node in converter station c, $\in [\underline{V^{\text{f}}_c}, \overline{V^{\text{f}}_c}], [\underline{\theta^{\text{f}}_c}, \overline{\theta^{\text{f}}_c}]$
$\lvert V_i\rvert, \theta_i$	Voltage at ac node i, $\in [\underline{V_i}, \overline{V_i}], [\underline{\theta_i}, \overline{\theta_i}]$
$I^{\text{cv,ac}}_c$	Converter ac-side current at station c, $\in [\pm\overline{I^{\text{cv,ac}}_c}]$
$I^{\text{cv,dc}}_c$	Converter dc-side current at station c, $\in [\pm\overline{I^{\text{cv,dc}}_c}]$
P_g	Active power of generator g, $\in [\underline{P_g}, \overline{P_g}]$

The work was supported in part by the CSIRO Strategic Project on Global Power System Transformation under Grant number: OD-223474 and in part by the International Clean Innovation Researcher Network Grant (OD-232814).
Author emails: ghulam.mohyuddin@csiro.au, rahmat.heidarihaei@csiro.au, frederik.geth@gridqube.com, hakan.ergun@kuleuven.be

$P_c^{\text{cv,dc}}$	Power on dc-side of converter c, $\in [\pm\overline{P_c^{\text{cv,dc}}}]$
$P_{def}^{\text{dc}}, P_{dfe}^{\text{dc}}$	Power flows in dc branch d between nodes $e \rightleftarrows f$, $\in [\pm\overline{P_d}]$
Q_g	Reactive power of generator g, $\in [\underline{Q_g}, \overline{Q_g}]$
$S_{cie}^{\text{pr}}, S_{cei}^{\text{pr}}$	Complex power flows in converter station c phase reactor between nodes $i \rightleftarrows e$, $\in [\pm\overline{S_c^{\text{pr}}}]$
$S_{cie}^{\text{tf}}, S_{cei}^{\text{tf}}$	Complex power flows in converter station c transformer between nodes $i \rightleftarrows e$, $\in [\pm\overline{S_c^{\text{tf}}}]$
$S_c^{\text{cv,ac}}$	Complex ac power of converter c, $\in [\pm\overline{S_c^{\text{cv,ac}}}]$
S_{lij}, S_{lji}	Complex power flows in ac branch l between node $i \rightleftarrows j$, $\in [\pm\overline{S_l}]$
t_{lij}, θ_{lij}	Tap setting of ac branch l from node $i \rightarrow j$, $\in [\underline{t_l}, \overline{t_l}], [\underline{\theta_l}, \overline{\theta_l}]$
V_e^{dc}	Voltage at dc node e, $\in [\underline{V_e}, \overline{V_e}]$
y_i^{sh}	Shunt admittance at node i, $\in [\underline{y_i^{\text{sh}}}, \overline{y_i^{\text{sh}}}]$

I. Introduction

The Australian National Electricity Market (NEM) operates one of the world's largest power grids, interconnecting five states and territories, through both HVAC and HVDC transmission systems [1]. As a large power system, the NEM has characteristics that may be surprising from the European or US perspective, for instance, there is no day-ahead electricity market. Since October 2021, the wholesale electricity *spot market* settlement period is 5 min., providing strong price signals for investment in faster response technologies. The NEM grid stretches about 5000 km north to south, includes HVDC interconnectors but lacks phase-shifting transformers, and has a total length of around 40 000 km of transmission lines and cables. Such a total is close to Germany's 35 000 km[1], which supplies more energy to more customers but over a smaller area. The NEM delivers more than 200 TWh/year to 10.7 million customers. Over recent years, the rollout of distributed PV and wind has been progressing at a pace of 250 W per year per capita, surpassing that of the European Union, the USA, Japan, and China by four to five times [2]. The generation capacity was about 65 GW in December 2021, at which time there was 14 GW of distributed PV. By mid 2023, the cumulative installed PV had risen to almost 32 GW[2]. Solar and wind are particularly popular in South Australia, where the total demand is supplied frequently from these variable sources *only* (Fig. 1).

Such changes in generation necessitate a paradigm shift in the reliability management of the network. The Australian National Electricity Rules set the power grid security principles, requiring the NEM to be operated such that it remains in a secure operating state following a single credible contingency event [4]. This requirement highlights the importance of N-1 security-constrained optimal power flow (SCOPF) problems in ensuring the power grid's reliability and secure operation in various real-time applications and planning studies.

[1] https://www.bmwk.de/Redaktion/EN/Artikel/Energy/electricity-grids-of-the-future-01.html

[2] https://pv-map.apvi.org.au/analyses

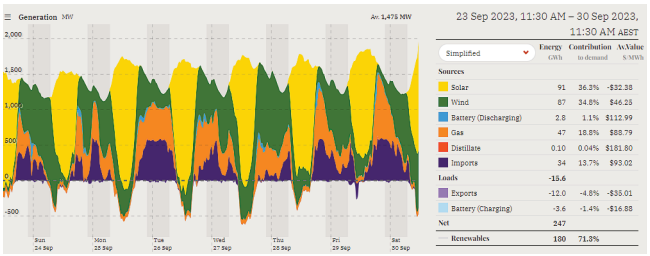

Fig. 1. South Australia frequently operates for more than 100% of local demand on renewables. Data: https://opennem.org.au/ [3]

A. Specifying the SCOPF Problem

SCOPF optimally configures and dispatches the power system in normal conditions (first stage - base case) to prevent steady-state operating conditions from exceeding emergency ratings following the occurrence of single credible contingency events (second stage - contingency cases). Most commonly, the N-1 SCOPF problem is considered, where N-1 refers to the failure of a single component at a time.

SCOPF problems pose significant computational challenges due to the scale, complexity, mathematical characteristics, and time-bound solution requirements for real-world grids. The NEM has about 2000 buses interconnected by HVAC and HVDC components with significant complexity, which necessitates advanced control and coordination strategies to manage power flows [5]. The computational burden further increases with a large number of contingencies as each contingency introduces a similar or even greater number of variables and constraints as present in the base case problem [6].

In terms of mathematical characteristics, the hybrid ac-dc power grid's physics is best represented by a nonlinear formulation, leading to a challenging non-convex, NP-hard optimization problem [7], [8]. Moreover, the contingency case model includes complementarity conditions related to power output limits for generators and voltage limits for HVDC converters [9], [10]. These complementarity conditions introduce additional nonlinearities and certain degeneracies to the model. Despite these challenges, operators need SCOPF solutions within stringent time constraints, typically less than 5 minutes, to support various real-time applications.

B. Review of SCOPF Models

The most common modeling approaches for SCOPF include two-stage mathematical programming problem (TSMP) [11], network compression [9], distributed optimization [12]–[14], machine learning [15]–[17], and decomposition [18], [19]. The TSMP uses complete models for both the base and contingency case optimization stages but the scalability of the problem remains a challenge for real-world power systems. To improve the scalability, in [20], contingency cases were linearized, and in [21], binding umbrella constraints in the 'dc'-approximation were identified to represent complete models. However, the problem remains an integrated TSMP problem. The network compression approach [9] identifies a limited area for each contingency called the active region. It keeps an

TABLE I
COMPUTATION AND AC FEASIBILITY IN LARGE-SCALE BENDERS DECOMPOSITION-BASED SCOPF FORMULATIONS [20]

Formulation	Features			
	Solvable	AC Feasible	AC Recovery	Optimality
NMNS	×	✓	×	×
NMLS	✓	✓	×	×
LMLS	✓	×	✓	✓

exact model for the active region and replaces the rest with an equivalent network. Despite being computationally efficient, incomplete models can result in sub-optimal solutions and may violate constraints. In distributed approaches, multi-agent-based Lagrangian multipliers [12] and alternating direction method of multipliers [13], [14] were presented that utilize the linear dc formulation and different relaxations of the real problem. However, these methods can not be utilized with the more accurate nonlinear formulation. Recently, some machine learning approaches were proposed including deep learning [15], deep reinforcement learning [16], and deep learning with knowledge graph [17]. However, there remains potential concerns regarding the implementation of these approaches [22].

SCOPF can also be decomposed into a master problem and several sub-problems, which interact iteratively. The advantages are that both master and sub-problems can be kept tractable, similar to optimizing a system only in a base or contingency case allowing distributed processing. Decomposition techniques such as Benders decomposition [18] or column and constraint generation [19] have been extensively applied to many industrial applications. However, it requires convexity of the feasible region, which cannot be guaranteed by a nonlinear formulation. Despite these challenges, an approach addressing nonlinear sub-problems was presented in [23]. However, it does not scale well and the optimality can not be guaranteed.

In [20], several SCOPF formulations are implemented using Benders decomposition, which include nonlinear master with non-linear sub-problem (NMNS), nonlinear master with linear sub-problem (NMLS), and linear master with linear sub-problem (LMLS) formulations and the trade-off between AC feasibility and computational efficiency is determined (Table I). The detailed analysis highlights that the NMLS model is both solvable and AC feasible, without necessitating an AC recovery solve in each iteration. This is because the master problem has the complete set of non-convex, non-linear constraints. The nonlinear formulations may not always yield globally optimal solutions due to the non-convex nature however, the optimal solutions obtained from LMLS model after AC recovery solve may also result in sub-optimality. Taking the benefit out of this research, several studies have utilised hybrid SCOPF models [9], [23].

C. Scope and Contributions

To address these limitations, this paper develops a decomposition scheme for the preventive SCOPF problem, with an emphasis on computational and practical aspects. Our unique decomposition approach distinguishes itself from prior methods [18], [19], [23]. In the master problem, a nonlinear formulation is considered for an integrated ac-dc power system that accounts for valid constraints for each contingency case. In the proposed decomposition scheme, only the optimization problem that is solved is the master problem with additional cutting planes and generator response constraints. The sub-problems are replaced by a (fast) *nonlinear ac-dc power flow solver* [24] to perform the feasibility checks and the cutting planes are added based on pre-processed structures such as power transfer distribution factors (PTDFs), line outage distribution factors (LODFs), dc distribution factors (DCDFs), and dc grid LODFs (dcLODFs). Based on feasibility checks, these factors are transformed into constraints (cutting planes that differ from Benders' cuts), which are added to master problem. These cutting planes represent the network for contingency cases.

Furthermore, our approach involves efficient contingency filtering, cyclic selection of filtered contingencies, careful choice of slack variables, and a tailored warm start to the nonlinear problem, which further improves the computation. The two prominent categories are severity index (SI) [25]–[27] and non-dominated contingency (NDC) based filters [28], [29]. The SI filter ranks contingencies using a SI calculated on a contingency-case power flow and selects those yielding a SI above a threshold. It requires tuning of thresholds and the size of the filtered subset. Thus the NDC filter is implemented, which selects a single contingency or a group as a minimal subset containing for each constraint a contingency that leads to the largest violation filtering out the dominated contingencies. Summarizing, the main contributions of this work are:

- The development of a new SCOPF model for real-world ac-dc grids combining a decomposition scheme, contingency ranking, evaluation, and non-dominated filtering algorithm, cyclic selection of filtered contingencies, careful choice of slack variables, and a tailored warm start to the nonlinear problem.
- Implementation of the proposed SCOPF methodology on the synthetic Australian NEM ac-dc power system in real-world scenarios.

The paper is structured as follows. Section II details the proposed SCOPF methodology and Section III, provides the mathematical formulation of the the proposed nonlinear ac-dc grid SCOPF model. Sections IV and V provide numerical experiments and conclusions.

II. PROPOSED SCOPF METHODOLOGY

The proposed methodology is illustrated in Fig. 2. In the first phase, a nonlinear ac-dc grid OPF problem (master problem with an empty contingency set) is solved to determine a base case operating point. Based on this operating point, Algorithm 1 ranks, evaluates, and filters non-dominated contingencies from the given contingency set. In the second phase, the NLP ac-dc SCOPF master problem is solved iteratively using the base-case operating point as a warm start to determine a secure operating point. Here the most severe contingencies are selected and the corresponding cutting planes are calculated

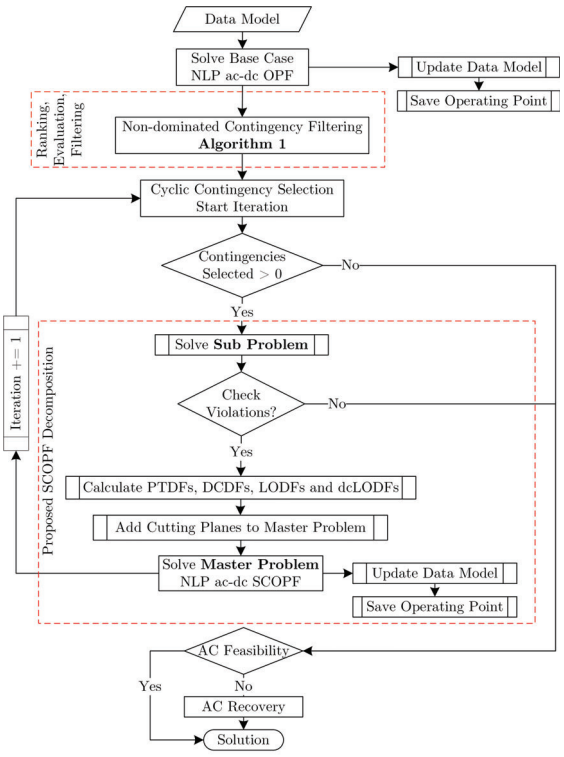

Fig. 2. Proposed workflow for the SCOPF in the Australian NEM ac-dc grid.

and added to the master problem during each iteration, inspired by the Benders decomposition.

A standard Benders decomposition requires a master problem that models system operation in the pre-contingency state and a sub-problem for each contingency stage. As large ac-dc grids may have several 1000s of lines and transformers, it takes a prohibitive amount of time just to implement the standard Benders decomposition algorithm. Therefore, the standard sub-problem is replaced by a *nonlinear ac-dc power flow solver* [24] to perform feasibility checks, and the proposed decomposition scheme explicitly identifies and includes only the cutting planes for the transmission lines and transformers whose capacities are violated. This strategic relaxation of the non-binding constraints (see section III-C) speeds up the process of obtaining a feasible solution. Note that these cutting planes are derived based on DC power flow assumptions.

III. AC-DC Grid SCOPF Model

A. Master problem

The master problem models the system operation in the pre-contingency state. The model includes a nonlinear static ac grid, the HVDC converter station supporting both voltage-source converter (VSC) and line-commutated converter (LCC) technologies, and the dc grid as shown in Fig. 3. The objective function is formulated as,

$$\min f(P_g) + \sum\nolimits_{k\in\mathcal{K}^g} \psi\, \varsigma_{g,k} + \sum\nolimits_{k\in\mathcal{K}^b} \psi\, \varsigma_{lij,k} + \sum\nolimits_{k\in\mathcal{K}^c} \psi\, \varsigma_{lij,k}. \quad (1)$$

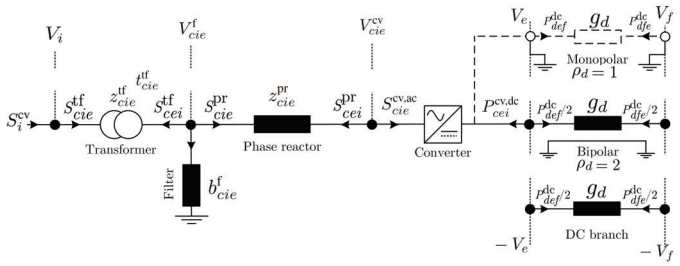

Fig. 3. The Overview of parameters and variables in converter station model.

Here, (1) minimizes the operation cost, where the generator cost function $f(P_g)$ supports both polynomial and piecewise linear cost functions and all slack violations $\varsigma_{lij,k}, \varsigma_{g,k}$, regardless of their type, conform to same significantly higher penalty cost ψ. The constraints are defined as follows.

$$S_{lij} = \left(y_l + y_{lij}^{sh}\right)^* \frac{|V_i|^2}{|t_{lij}|^2} - y_l^* \frac{V_i V_j^*}{t_{lij}}, \forall lij \in \mathcal{T}^{\text{ac}} \quad (2)$$

$$S_{lji} = \left(y_l + y_{lji}^{sh}\right)^* |V_j|^2 - y_l^* \frac{V_i^* V_j}{t_{lij}^*}, \forall lji \in \mathcal{T}^{\text{ac,r}} \quad (3)$$

$$\underline{\delta\theta_{lij}} \le \angle(V_i V_j^*) \le \overline{\delta\theta_{lij}}, \forall lij \in \mathcal{T}^{\text{ac}} \quad (4)$$

$$|S_{lij}| \le \overline{S_l}, \forall lij \in \mathcal{T}^{\text{ac}} \cup \mathcal{T}^{\text{ac,r}} \quad (5)$$

$$|S_{lij}| \le |V_i|\overline{I_{lij}}, \forall lij \in \mathcal{T}^{\text{ac}} \cup \mathcal{T}^{\text{ac,r}} \quad (6)$$

$$\angle V_r = 0, \quad \forall r \in \mathcal{R}. \quad (7)$$

$$S_{cie}^{\text{tf}} = y_c^{\text{tf}*} \frac{|V_i|^2}{t_c^2} - y_c^{\text{tf}*} \frac{V_i V_c^{\text{f}*}}{t_c}, \forall cie \in \mathcal{T}^{\text{cv}} \quad (8)$$

$$S_{cei}^{\text{tf}} = y_c^{\text{tf}*} |V_c^{\text{f}}|^2 - y_c^{\text{tf}*} \frac{V_i^* V_c^{\text{f}}}{t_c}, \forall cie \in \mathcal{T}^{\text{cv,r}} \quad (9)$$

$$\Im(S_c^{\text{f}}) = -b_c^{\text{f}} |V_c^{\text{f}}|^2, \forall cie \in \mathcal{T}^{\text{cv}} \quad (10)$$

$$S_{cie}^{\text{pr}} = y_c^{\text{pr}*} |V_c^{\text{f}}|^2 - y_c^{\text{pr}*} V_c^{\text{f}} V_c^{\text{cv}*}, \forall cie \in \mathcal{T}^{\text{cv}} \quad (11)$$

$$S_{cei}^{\text{pr}} = y_c^{\text{pr}*} |V_c^{\text{cv}}|^2 - y_c^{\text{pr}*} V_c^{\text{f}*} V_c^{\text{cv}}, \forall cie \in \mathcal{T}^{\text{cv,r}} \quad (12)$$

$$S_{cei}^{\text{tf}} + S_{cie}^{\text{pr}} + \Im(S_c^{\text{f}}) = 0, \forall cie \in \mathcal{T}^{\text{cv}} \quad (13)$$

$$|S_c^{\text{cv,ac}}| \le \overline{S_c^{\text{cv,ac}}}, \forall cie \in \mathcal{T}^{\text{cv}} \quad (14)$$

$$|I_c^{\text{cv,ac}}| \le \overline{I_c^{\text{cv,ac}}}, \forall cie \in \mathcal{T}^{\text{cv}} \quad (15)$$

$$|S_c^{\text{cv,ac}}| = |V_c^{\text{cv}}||I_c^{\text{cv,ac}}|, \forall cie \in \mathcal{T}^{\text{cv}} \quad (16)$$

$$P_c^{\text{cv,loss}} = a_c^{\text{cv}} + b_c^{\text{cv}} |I_c^{\text{cv,ac}}| + c_c^{\text{cv}} |I_c^{\text{cv,ac}}|^2, \forall cie \in \mathcal{T}^{\text{cv}} \quad (17)$$

$$P_c^{\text{cv,ac}} + P_c^{\text{cv,dc}} = P_c^{\text{cv,loss}}, \forall cie \in \mathcal{T}^{\text{cv}} \quad (18)$$

$$P_c^{\text{cv,dc}} = V_e^{\text{dc}} I_c^{\text{cv,dc}}, \forall cie \in \mathcal{T}^{\text{cv}} \quad (19)$$

$$P_c^{\text{cv,ac}} = \cos\varphi_c \overline{S_c^{\text{cv,ac}}}, \forall cie \in \mathcal{T}^{\text{cv}} \quad (20)$$

$$Q_c^{\text{cv,ac}} = \sin\varphi_c \overline{S_c^{\text{cv,ac}}}, \forall cie \in \mathcal{T}^{\text{cv}} \quad (21)$$

$$P_{def}^{\text{dc}} = \rho_d g_d^{\text{s}} V_e^{\text{dc}} (V_e^{\text{dc}} - V_f^{\text{dc}}), \forall def \in \mathcal{T}^{\text{dc}} \quad (22)$$

$$P_{dfe}^{\text{dc}} = \rho_d g_d^{\text{s}} V_f^{\text{dc}} (V_f^{\text{dc}} - V_e^{\text{dc}}), \forall dfe \in \mathcal{T}^{\text{dc,r}} \quad (23)$$

$$\sum_{cie\in\mathcal{T}^{\text{cv}}} P_c^{\text{cv,dc}} + \sum_{def\in\mathcal{T}^{\text{dc}}} P_{def}^{\text{dc}} = \sum_{me\in\mathcal{T}^{\text{l,dc}}} P_m, \forall e \in \mathcal{E} \quad (24)$$

$$\sum_{gi\in\mathcal{T}^{\text{g}}} P_g - \sum_{mi\in\mathcal{T}^{\text{l,ac}}} P_m - \Re(y_i^{\text{sh,f}} + y_i^{\text{sh}})^* |V_i|^2 = \sum_{cie\in\mathcal{T}^{\text{cv}}} P_{cie}^{\text{tf}} + \sum_{lij\in\mathcal{T}^{\text{ac}}} P_{lij}, \forall i \in \mathcal{N} \quad (25)$$

$$\sum_{gi\in\mathcal{T}^{\text{g}}} Q_g - \sum_{mi\in\mathcal{T}^{\text{l,ac}}} Q_m - \Im(y_i^{\text{sh,f}} + y_i^{\text{sh}})^* |V_i|^2 = \sum_{cie\in\mathcal{T}^{\text{cv}}} Q_{cie}^{\text{tf}} + \sum_{lij\in\mathcal{T}^{\text{ac}}} Q_{lij}, \forall i \in \mathcal{N} \quad (26)$$

The ac branch complex power flows S_{lij}, S_{lji}, for branch l connecting nodes i and j, are modeled using complex quantities for node voltage V_i and branch series admittance y_l in (2) and (3). Here y_l, y_{lij}^{sh}, and y_{lji}^{sh} are π-model parameters and t_{lij} is complex transformation ratio variable. Moreover, $S_{lij} = P_{lij} + \text{j}Q_{lij}$. Here, the bounds on angle difference $\angle(V_i V_j^*)$ between two nodes i and j are enforced in (4). Moreover, the thermal limit $\overline{S_{lij}}$ and current limit $\overline{I_{lij}}$ of ac branch flow are enforced in (5) and (6) respectively. Finally, the reference node voltage angle $\angle V_r$ is set to zero as in (7).

The dc converter transformer transforms the ac node voltage V_i to a suitable level V_c^{f}, which is the internal voltage at the filter node of the converter station c. The complex power flow $S_{cie}^{\text{tf}}, S_{cei}^{\text{tf}}$ through the transformer of a converter station c connecting an ac grid node i with a dc grid node e are expressed in (8) and (9). Here, S_{cie}^{tf} is defined as $P_{cie}^{\text{tf}} + \text{j}Q_{cie}^{\text{tf}}$. The reactive power of the filter capacitor with susceptance b_c^{f} is defined in (10). Next, the complex power flow $S_{cie}^{\text{pr}}, S_{cei}^{\text{pr}}$ through the phase reactor with admittance y_c^{pr} is expressed in (11) and (12). Ultimately, the balance between the converter transformer, phase reactor, and filter is expressed in (13). The converter ac-side apparent power and current limits are enforced in (14) and (15), respectively. The converter's ac-side complex power $S_c^{\text{cv,ac}}$ is defined as $P_c^{\text{cv,ac}} + \text{j}Q_c^{\text{cv,ac}}$. Moreover, the converter's ac-side apparent power and losses are defined in (16) and (17). The ac- and dc-sides are linked by the losses as in (18), whereas, the converter dc-side power is defined in (19). Finally, the predetermined relationship between the active and reactive power of LCC converters is outlined in (20) and (21), respectively.

The dc grid power flows P_{def}^{dc}, P_{dfe}^{dc} are divided by the number of poles ρ_d, e.g. two. For monopolar dc configurations, the entire flow goes through a single conductor, thus $\rho_d = 1$. Based on the bus injection model of a dc line d connecting nodes e and f, the power flow on the dc line with conductance g_d^{s} and the nodal voltages V_e^{dc} and V_e^{dc} are expressed in (22) and (23). Finally, the dc grid nodal power balance at a node e is enforced in (24) and the ac nodal real and imaginary power balance at a node i is enforced in (25) and (26).

B. Sub-Problem Contingency Case

The sub-problems assess the feasibility for each contingency, to ensure that the master problem satisfies all operational constraints. To perform the feasibility check, slack variables $\varsigma_{lij,k}^S$ are introduced for the operational constraints, and the following optimization problem is solved for each contingency k:

$$\Phi = \min \sum_{k\in\mathcal{K}} \varsigma_{lij,k}^S. \quad (27)$$

$$P_{lij,k} = \sum_{j\in\mathcal{N}} \chi_{ij}^{\text{ptdf}} \Big(\sum_{gj\in\mathcal{T}_k^{\text{g}}} P_{g,k} - \sum_{mj\in\mathcal{T}^{\text{l,ac}}} P_{m,k} - \Re(y_j^{\text{sh,f}} + y_{lij}^{\text{sh}}) |\widehat{V_j}|^2 - \chi_j^{\text{lf}} P^{\text{loss}} \Big) + \sum_{e\in\mathcal{E}} \chi_{ie}^{\text{dcdf}} P_{cie,k}^{\text{tf}}, \forall lij \in \mathcal{T}^{\text{ac}}, \quad (28)$$

$$P_{lji,k} = \sum_{j\in\mathcal{N}} \chi_{ij}^{\text{ptdf}} \Big(\sum_{gj\in\mathcal{T}^{\text{g}}} P_{g,k} - \sum_{mj\in\mathcal{T}^{\text{l,ac}}} P_{m,k} - \Re(y_j^{\text{sh,f}} + y_{lji}^{\text{sh}}) |\widehat{V_j}|^2 - \chi_j^{\text{lf}} P^{\text{loss}} \Big) + \sum_{e\in\mathcal{E}} \chi_{ie}^{\text{dcdf}} P_{cei,k}^{\text{tf}}, \forall lji \in \mathcal{T}^{\text{ac,r}}, \quad (29)$$

$$-\overline{S_l} - \varsigma_{lij,k}^S \geq P_{lij} \leq \overline{S_l} + \varsigma_{lij,k}^S, \forall lij \in \mathcal{T}^{\text{ac}} \cup \mathcal{T}^{\text{ac,r}}, \quad (30)$$

$$P_{cie,k}^{\text{tf}} = -\frac{\Im(y_c^{\text{tf}})}{t_c}(\theta_{i,k} - \theta_{c,k}^{\text{f}}), \forall cie \in \mathcal{T}^{\text{cv}}, \quad (31)$$

$$P_{cei,k}^{\text{tf}} = -\frac{\Im(y_c^{\text{tf}})}{t_c}(\theta_{c,k}^{\text{f}} - \theta_{i,k}), \forall cie \in \mathcal{T}^{\text{cv,r}}, \quad (32)$$

$$P_{cie,k}^{\text{pr}} = -\Im(y_c^{\text{pr}})(\theta_{c,k}^{\text{f}} - \theta_{c,k}^{\text{cv}}), \forall cie \in \mathcal{T}^{\text{cv}}, \quad (33)$$

$$P_{cei,k}^{\text{pr}} = -\Im(y_c^{\text{pr}})(\theta_{c,k}^{\text{cv}} - \theta_{c,k}^{\text{f}}), \forall cie \in \mathcal{T}^{\text{cv,r}}, \quad (34)$$

$$P_{c,k}^{\text{cv,ac}} + P_{c,k}^{\text{cv,dc}} = a_c^{\text{cv}} + b_c^{\text{cv}} P_{c,k}^{\text{cv,ac}}, \forall cie \in \mathcal{T}^{\text{cv}}, \quad (35)$$

$$\sum_{gi\in\mathcal{T}^{\text{g}}} P_{g,k} - \sum_{mi\in\mathcal{T}^{\text{l,ac}}} P_{m,k} - \Re(y_i^{\text{sh,f}} + y_{lij}^{\text{sh}}) |\widehat{V}_i|^2 = \sum_{cie\in\mathcal{T}^{\text{cv}}} P_{cie,k}^{\text{tf}} + \sum_{lij\in\mathcal{T}^{\text{ac}}} P_{lij,k}, \forall i \in \mathcal{N}, \quad (36)$$

$$\sum_{cie\in\mathcal{T}^{\text{cv}}} P_{c,k}^{\text{cv,dc}} + \sum_{def\in\mathcal{T}^{\text{dc}}} P_{def,k}^{\text{dc}} = \sum_{me\in\mathcal{T}^{\text{l,dc}}} P_{m,k}, \forall i \in \mathcal{N}, \quad (37)$$

$$\boldsymbol{P}_{g,k} = \widehat{\boldsymbol{P}}_g : \boldsymbol{\lambda}_k, \forall g \in \mathcal{G}, \quad (38)$$

$$\boldsymbol{P}_{cie,k}^{\text{tf}} = \widehat{\boldsymbol{P}}_{cie}^{\text{tf}} : \boldsymbol{\mu}_k, \forall cie \in \mathcal{T}^{\text{cv}} \quad (39)$$

The objective function in (27) minimizes the line flow violations captured by the slack variables. The ac grid power balance is enforced in (36). The ac branch flows are defined in terms of the PTDF and DCDF matrices χ_{ij}^{ptdf} and χ_{ie}^{dcdf} in (28) and (29) [30]. The ac grid losses are determined using loss factors χ_i^{lf} [31]. The converter station transformer and phase reactor power flows are defined in (31), (32), (33), and (34). The converter ac- and dc-sides are linked through losses as expressed in (35). Here, all the voltage magnitudes in ac as well as dc networks are assumed as 1 pu, whereas in (36), (28) and (29) the voltage magnitude $|\widehat{V_j}|^2$ has the same value as the base case solution. The converter's dc-side injections constitute the dc branch power flows and the dc grid power balance is enforced in (37). The ac branch flows are relaxed as

in (30). Moreover, the ac-dc power system bounds of decision variables are enforced as in the master problem. Generators active power $\widehat{\boldsymbol{P}}_g$ and converter stations ac grid injection $\widehat{\boldsymbol{P}}^{\text{tf}}_{cie}$ are set to the solutions of the master problem in (38) and (39) with the corresponding dual variables $\boldsymbol{\lambda}_k$ and $\boldsymbol{\mu}_k$. If sub-problem's objective value is non-zero, the master problem's solution does not satisfy the constraints, and the Bender's cuts

$$\Phi + \boldsymbol{\lambda}_k\big[\boldsymbol{P}_{g,k} - \widehat{\boldsymbol{P}}_g\big] - \boldsymbol{\mu}_k\big[\boldsymbol{P}^{\text{tf}}_{cie,k} - \widehat{\boldsymbol{P}}^{\text{tf}}_{cie}\big] \leq 0 \tag{40}$$

are added to the master problem. This process is iterated for all contingencies, and the corresponding sub-problem is updated with the new master problem solution in each iteration.

C. Strategic Implementation of Sub-Problems

We replace the sub-problems by a fast *nonlinear ac-dc power flow solver* [24] to perform feasibility checks using the updated starting point from master problem. In case of branch flow violations, the cutting planes are identified, explicitly calculated, and added to the master problem corresponding to each contingency. Note that these cutting planes are derived based on DC power flow assumptions.

1) AC Branch Contingency: In case of an ac branch contingency, the cutting planes are defined as in (41), where for contingency states a correction is performed to the power flow of branch lij by considering the element $\chi^{\text{lodf}}_{ii(k)}$ of the LODF matrix and the row $i(k)$ of the PTDF matrix for the outage of ac branch $li(k)j$,

$$\begin{aligned}
&-\varsigma_{lij,k} - \overline{S_{lij}} \leq \\
&\quad \sum\nolimits_{j\in\mathcal{N}} \chi^{\text{ptdf}}_{ij}\Big(\sum\nolimits_{gj\in\mathcal{T}^{\text{g}}} P_{g,k} - \sum\nolimits_{mj\in\mathcal{T}^{\text{l,ac}}} P_{m,k} \\
&\quad - \Re(y^{\text{sh,f}}_{j} + y^{\text{sh}}_{lij})|\widehat{V_j}|^2 - \chi^{\text{lf}}_{j} P^{\text{loss}}\Big) + \sum\nolimits_{e\in\mathcal{E}} \chi^{\text{dcdf}}_{ie} P^{\text{tf}}_{cie,k} \\
&+ \chi^{\text{lodf}}_{ii(k)} \sum\nolimits_{j\in\mathcal{N}} \chi^{\text{ptdf}}_{i(k)j}\Big(\sum\nolimits_{gj\in\mathcal{T}^{\text{g}}} P_{g,k} - \sum\nolimits_{mj\in\mathcal{T}^{\text{l,ac}}} P_{m,k} \\
&- \Re(y^{\text{sh,f}}_{j} + y^{\text{sh}}_{li(k)j})|\widehat{V_j}|^2 - \chi^{\text{lf}}_{j} P^{\text{loss}}\Big) + \sum\nolimits_{e\in\mathcal{E}} \chi^{\text{dcdf}}_{i(k)e} P^{\text{tf}}_{i(k)e,k} \\
&\qquad\qquad \leq \overline{S_{lij}} + \varsigma_{lij,k}.
\end{aligned} \tag{41}$$

2) DC Converter Contingency: For a dc converter contingency, the cutting planes are defined as in (42), where for contingency states a correction is performed to the power flow of branch lij via considering the element $\chi^{\text{dclodf}}_{ie(k)}$ of the dc grid dcLODF matrix and the row $e(k)$ of the DCDF matrix for the outage of the dc converter $cie(k)$,

$$\begin{aligned}
&-\varsigma_{lij,k} - \overline{S_{lij}} \leq \\
&\quad \sum\nolimits_{j\in\mathcal{N}} \chi^{\text{ptdf}}_{ij}\Big(\sum\nolimits_{gj\in\mathcal{T}^{\text{g}}} P_{g,k} - \sum\nolimits_{mj\in\mathcal{T}^{\text{l,ac}}} P_{m,k} \\
&- \Re(y^{\text{sh,f}}_{j} + y^{\text{sh}}_{lij})|\widehat{V_j}|^2 - \chi^{\text{lf}}_{j} P^{\text{loss}}\Big) + \sum\nolimits_{e\in\mathcal{E}} \chi^{\text{dcdf}}_{ie} \Re(S^{\text{tf}}_{cie,k}) \\
&\qquad + \chi^{\text{dclodf}}_{ee(k)} \sum\nolimits_{e\in\mathcal{E}} \chi^{\text{dcdf}}_{ie(k)} P^{\text{tf}}_{cie(k),k} \leq \overline{S_{lij}} + \varsigma_{lij,k}.
\end{aligned} \tag{42}$$

3) Generator Contingency: Some of the generators respond to the contingencies based on their offline participation factor α_g, while some have fixed output. The responding generator's active power injection is,

$$P^{\text{cont}}_{g,k} = P_{g,k} + \alpha_g \frac{P^{\text{out}}_{g,k}}{\sum_{g\in\mathcal{T}^g_k}\alpha_g}, \forall g \in \mathcal{T}^g_k, \tag{43}$$

Here, non-responding generators' output remains unchanged as,

$$P^{\text{cont}}_{g,k} = P_{g,k}, \forall g \in \mathcal{T}^g \cap \mathcal{T}^g_k, \tag{44}$$

Additionally, a slack variable is added to account for the capacity violation of responding generators as,

$$\varsigma_{g,k} + \sum\nolimits_{g\in\mathcal{T}^g_k} (\overline{P_g} - P_{g,k}) \geq P^{\text{out}}_{g,k}, \forall g \in \mathcal{T}^g_k, \tag{45}$$

Finally, the cutting planes responding to a generator contingency are formulated as,

$$\begin{aligned}
&-\varsigma_{lij,k} - \overline{S_{lij}} \leq \sum\nolimits_{j\in\mathcal{N}} \chi^{\text{ptdf}}_{ij}\Big(\sum\nolimits_{gj\in\mathcal{T}^{\text{g}}_k} P^{\text{cont}}_{g,k} \\
&\quad - \sum\nolimits_{mj\in\mathcal{T}^{\text{l,ac}}} P_{m,k} - \Re(y^{\text{sh,f}}_{j} + y^{\text{sh}}_{lij})|\widehat{V_j}|^2 - \chi^{\text{lf}}_{j} P^{\text{loss}}\Big) \\
&\qquad + \sum\nolimits_{e\in\mathcal{E}} \chi^{\text{dcptdf}}_{ie} P^{\text{tf}}_{cie,k} \leq \overline{S_{lij}} + \varsigma_{lij,k}.
\end{aligned} \tag{46}$$

Note that the slack variables $\varsigma_{lij,k}, \varsigma_{g,k}$ were carefully introduced only for the cutting planes to keep the variables at a minimum. They are non-zero bounded variables.

D. Contingency Ranking, Evaluation, Filtering

Identifying and evaluating contingencies is a crucial step in ensuring the reliability and security of a power system. Evaluating all contingencies is time-consuming and therefore, we prioritize the most important ones. The process in Algorithm 1 starts with ranking initial subsets of the contingency set $\mathcal{K}$, that is $\mathcal{K}^g$, $\mathcal{K}^b$, and $\mathcal{K}^c$ (respectively, generator, ac branch, and converter contingencies), with respect to maximum capacity loss and impedance of ousted components. The algorithm then combines this candidate list with the generator, ac branch, and converter ranking values to create an initial prioritized list of contingencies.

To evaluate, each contingency is embedded into the input data set $\mathbf{D}$, and based on the base case solution, the power flow is solved. The solution is checked for violations and the respective violation variables $\varsigma_{g,k}, \varsigma_{lij,k}, \varsigma_{cie,k}$ are updated. The contingency filtering relies on violations indicated by violation variables. However, selecting contingencies solely based on their highest violation values can result in redundant inclusions. This is because addressing constraints linked to one contingency can indirectly resolve constraints from other contingencies, i.e. it is dominated by the former contingency. Therefore, the proposed algorithm filters initially, based on the SI (constraint violation thresholds ϵ_f), if the violations are negligible then based on the maximum violation NDC criteria.

In [32], *individually NDCs* are proposed to identify redundant contingencies based on constraint violations. This approach enforces the constraints associated with all contingencies that are not individually dominated. This means that if they are dominated by other contingencies, their constraints

Algorithm 1 Contingency Ranking, Evaluation, Filtering

Inputs: $[\mathbf{D}:\mathbf{n}\rightarrow\mathbf{v}], [\boldsymbol{V}_i, \boldsymbol{S}_g, \boldsymbol{S}^{\text{tf}}_{cie}], [\mathcal{K}]$.
rank {generator contingencies} by $\max|\overline{S_g}|, \forall \mathcal{K}^{\text{g}} \subset \mathcal{K}$
rank {branch contingencies} by $\max|z_{lij}|, \forall \mathcal{K}^{\text{b}} \subset \mathcal{K}$
rank {converter contingencies} by $\max|\overline{S^{\text{cv,ac}}_{cie}}|, \forall \mathcal{K}^{\text{c}} \subset \mathcal{K}$

initialize {violation slacks} $\varsigma^{\text{p}}_{g,k}, \varsigma^{\text{q}}_{g,k}, \varsigma^{\text{s}}_{lij,k}, \varsigma^{\text{cv}}_{cie,k} \leftarrow 0, \forall k$
  for $k \in \mathcal{K}$, **do**
    update $\mathbf{D}^k = [\mathbf{D}[\mathbf{n}\rightarrow\mathbf{v}](x) = \emptyset,\ x = k?\ \mathbf{D}(x)]$
    if $\mathcal{T}^g \setminus \mathcal{T}^g_k \neq \emptyset$, **then**
      solve acdcpf$(\mathbf{D}^k, \boldsymbol{V}_i, \boldsymbol{S}_g, \boldsymbol{S}^{\text{tf}}_{cie}) \implies$ **sol**
      check violation(**sol**) $\implies \varsigma^{\text{p}}_{g,k}, \varsigma^{\text{q}}_{g,k}, \varsigma^{\text{s}}_{lij,k}, \varsigma^{\text{cv}}_{cie,k}$
    elseif $\mathcal{T}^{\text{ac}} \setminus \mathcal{T}^{\text{ac}}_k \neq \emptyset$, **then**
      solve acdcpf$(\mathbf{D}^k, \boldsymbol{V}_i, \boldsymbol{S}_g, \boldsymbol{S}^{\text{tf}}_{cie}) \implies$ **sol**
      check violation(**sol**) $\implies \varsigma^{\text{p}}_{g,k}, \varsigma^{\text{q}}_{g,k}, \varsigma^{\text{s}}_{lij,k}, \varsigma^{\text{cv}}_{cie,k}$
    elseif $\mathcal{T}^{\text{cv}} \setminus \mathcal{T}^{\text{cv}}_k \neq \emptyset$, **then**
      solve acdcpf$(\mathbf{D}^k, \boldsymbol{V}_i, \boldsymbol{S}_g, \boldsymbol{S}^{\text{tf}}_{cie}) \implies$ **sol**
      check violation(**sol**) $\implies \varsigma^{\text{p}}_{g,k}, \varsigma^{\text{q}}_{g,k}, \varsigma^{\text{s}}_{lij,k}, \varsigma^{\text{cv}}_{cie,k}$
    endif
    update $\mathbf{D}^k = \mathbf{D}[\mathbf{n}\rightarrow\mathbf{v}]$
  endfor

  for $k \in \mathcal{K}$, **do**
    if $(\varsigma_{ki} > \epsilon_f)||...||(\varsigma_{kN} > \epsilon_f)$, where, $\varsigma_{ki} = \sum_i \varsigma_{ki}$
    update $\widehat{\mathcal{K}} \leftarrow k$, **set** $k \in \mathcal{K} \setminus \widehat{\mathcal{K}}$
    endif
  endfor
  for $k \in \widehat{\mathcal{K}}$, **do**
    if $(\widehat{i}_k == \widehat{i}_j) \wedge (\widehat{\varsigma}_{ki} > \widehat{\varsigma}_{ji})$, where,
      $\widehat{\varsigma_{ki}} = \max\{\varsigma_{ki}\}, \widehat{\varsigma}_{ji} = \max\{\varsigma_{ji}\}, \forall k, j \in \widehat{\mathcal{K}}$, **then**
     update $\widehat{\mathcal{K}} \leftarrow k$, **set** $k \in \widehat{\mathcal{K}} \setminus \widehat{\mathcal{K}}$
    endif
  endfor
  sort contingency set $\{\forall k \in \widehat{\mathcal{K}}\}$ by $\max\{\sum_i^N \varsigma_{ki}\}$
return: contingency set $\{\forall k \in \widehat{\mathcal{K}}\}$

can be implicitly satisfied by enforcing constraints associated with more critical contingencies. This approach, however, is too conservative. In our algorithm, only the most severely violated constraint $\widehat{i}_k$ with the corresponding violation $\widehat{\varsigma}_{ki}$ for each contingency k is considered, rather than all the constraints to avoid selection of maximum violation-dominated contingencies.

IV. Numerical Results

In this section, we present the comparison of the proposed SCOPF model with the conventional multi-period TSMP model on four smaller cases, to serve as a validation of the proposed methodology. Next, we focus on the application to the NEM system, which cannot be solved using the TSMP approach.

A. Data and Computational Setup

The data of the four test cases `case5`, `case24`, `case67`, `case500` used for validation purpose is available at [33].

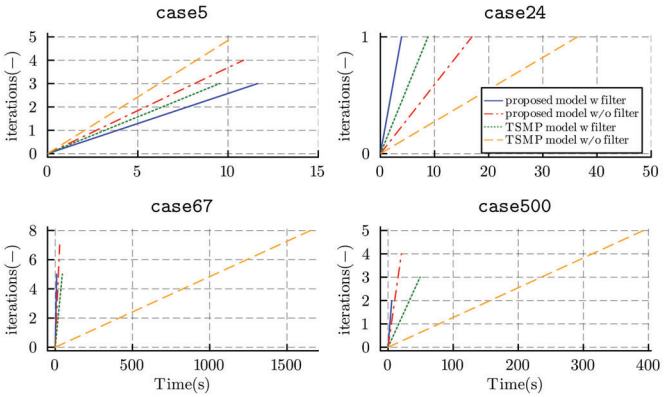

Fig. 4. Number of iterations versus computation time for preventive solutions.

Furthermore, the synthetic NEM data set is used in this study, which was initially released as `S-NEM2000` [1]. `S-NEM2000` has 2000 ac buses, 1324 ac lines, 1418 two-winding transformers, 113 three-winding transformers, 261 generators, 301 shunts, and 1702 loads. Later, HVDC inter-connectors such as Basslink, Murraylink, and Directlink (Table III) are added to `S-NEM2000` [24]. This includes 6 dc buses, 6 converter stations, and 5 dc transmission lines. This new version `S-NEM2000_acdc` is also made publicly available[3]. In this study, we consider a total of 3081 ac lines and transformers, 6 converters, and 298 generator contingencies.

The IPOPT solver (v1.2.0) is used to solve the SCOPF models on a PC with Intel Core i9-11950H with 64 GB of RAM. The TSMP and the proposed ac-dc SCOPF are available in the open-source library 'PowerModelsACDCsecurityconstrained.jl' [1].

B. Comparison of Proposed SCOPF Model with TSMP Model

Four test cases `case5`, `case24`, `case67`, `case500` are solved using the proposed and TSMP models, and the results are presented in Table II. The percentage gap in the preventive operation cost between the TSMP and the proposed model is 0.05%, 0.06%, 0.7%, and 0.65% in each case respectively. The difference between the base case and the preventive solution indicates the security cost. The security costs from TSMP and the proposed model are an additional 26.29%, 0%, 0.29%, 17.79% and 26.35%, 0%, 0.98%, 18.56% on top of the base case operation cost in each case respectively. The same contingencies are secured by the proposed and TSMP models. However, for `case5`, generator 2, and ac branches 1-3 remain unsecured. Both the generator 2 and branch 1-3 contingency violate ac branch 1-2 thermal rating by 0.29 pu and 0.26 pu respectively. This happens because in both of these contingencies, only branch 1-2 has to carry the compensation power to either of the ends. For `case24` all the contingencies are secure at the base operating point. Similarly, for `case67`, ac branches between buses 35-36, 35-47, 36-38, 44-48, 45-46, 58-61, and converter 9 are unsecured.

[3] https://github.com/csiro-energy-systems/Synthetic-NEM-2000bus-Data

TABLE II
COMPARISON OF TSMP AND PROPOSED AC-DC SCOPF MODELS

Case	TSMP model						Proposed Model			
	N-1 contingencies (k)	Base objective ($/h)	Preventive objective ($/h)	N-1 unsecure (k)	Time w filter (s)	Time w/o filter (s)	Preventive objective ($/h)	N-1 unsecure (k)	Time w filter (s)	Time w/o filter (s)
case5	2g, 7bac, 3cdc	193.90	244.88	1g, 1bac	9.53217	10.3112	245.007	1g, 1bac	10.9992	10.8575
case24	65g, 77bac, 7cdc	1.54886e5	1.54886e5	-	8.78343	36.4080	1.54886e5	-	3.90513	16.9051
case67	20g, 102bac, 9cdc	1.22877e5	1.23242e5	6bac,1cdc	46.3624	1653.01	124092.0	6bac, 1cdc	9.52787	28.9969
case500	51g, 326bac, 10cdc	27602.4	32513.9	1bac	49.2133	392.327	32725.5	1bac	5.70389	20.5215

Finally, for case500, the ac branch between buses 246 to 247 is unsecured. These unsecured contingencies can be secured using corrective actions.

The important aspect is the computation time where the proposed approach solves the SCOPF faster than the TSMP model. The average computation time versus the number of iterations for each case with and without NDC filtering, using the TSMP and proposed model is shown in Fig. 4. As can be seen, for case24, case67, and case500, the proposed model substantially decreases the computation time for the SCOPF problem due to the efficient modeling approach and NDC filtering method. We note that the TSMP model runs into a memory limit as the model keeps on growing as the number of contingencies increases and the solver takes a prohibitive amount of time to solve the problem.

C. Proposed SCOPF model on S-NEM2000acdc

To evaluate the efficacy of the proposed ac-dc SCOPF model on S-NEM2000acdc, four different scenarios have been considered: (1) benchmark; (2) high load; (3) minimum load; and (4) high load, renewable energy zones, and new point-to-point and meshed HVDC links integration. The results are shown in Table IV.

- In scenario 1, the security cost is an additional 6.28% to the base operation cost. The proposed SCOPF eliminated the line loading violations on ac lines as shown in Fig. 8. However, the violations due to 3 generator and 7 ac branch contingencies can not be eliminated by the preventive solution.
- In scenario 2, a higher number of violations are observed including the Basslink between Victoria and Tasmania (Fig. 9). The preventive solution eliminates these violations except for 1 generator, and 6 ac line contingencies allowing minimal line-loading violations since too many lines have their limits binding. These minimal violations are captured by the slack variables in the objective as additional penalties, which are set at higher values such as 5E5. Therefore, the preventive solution operation cost is 1978.37 $/h, and the penalty cost is 16 030.63 $/h. The total violation is 0.032 pu. These violations can be eliminated by corrective actions. The security cost in scenario 2 is an additional 26.01% to the base operation cost.
- In scenario 3, fewer violations are observed and the same contingencies are secured at an additional security cost of 11.73% as in scenario 1.
- In scenario 4, 36 renewable energy zones, 2 point-to-point, and 3 HVDC links in meshed configuration are added and the SCOPF is solved at a high load. A large number of line loading violations are observed as shown in Fig. 10. The proposed model eliminated most of the violations except for a few ac line loading violations caused by the 2 generator and 22 ac line contingencies. The preventive solution operation cost is 1564.53 $/h, and the penalty cost is 10790.47 $/h with a total violation of 0.021 pu. The security cost in this scenario is 12.31 % in addition to base case.

The normalized ac-dc line and generator-converter loadings in each scenario for the base case and preventive solutions using the proposed model are shown in Fig. 5 and Fig. 6 respectively. The ac-dc voltage magnitude in each scenario for the base case and preventive solutions is shown in Fig. 7.

The proposed model efficiently solves the ac-dc SCOPF for the S-NEM2000_acdc within 5 min, which aligns with the real-time NEM operation window. This enables the use of SCOPF for real-time applications and extensive planning tasks, where quick and accurate solutions are crucial. Computation can be sped up further by paralleling the sub-problems.

TABLE III
HVDC INTERCONNECTORS ADDED TO S-NEM2000

Name	Components					
	ac buses (indexes)	converter stations TF	converter stations filter	converter stations reactor	dc buses (-)	dc lines (-)
Bass	1004,1507	✓	×	✓	2	1
Murray	21,876	✓	×	✓	2	3
Direct	734,1919	✓	×	✓	2	1

TABLE IV
S-NEM2000ACDC RESULTS USING PROPOSED AC-DC SCOPF MODEL

Scenario	Base objective x10^2($/h)	Preventive objective x10^2 ($/h)	N-1 unsecure (k)	Iter. (-)	Time (s)
1	1026.71	1091.29	3g, 7bac	9	298.154
2	1569.89	1.8009e4	1g, 6bac	11	256.441
3	650.277	726.596	3g, 7bac	8	295.681
4	1392.95	1.2355e4	2g, 22bac	10	302.5

V. CONCLUSIONS

This paper presents a new methodology to efficiently solve the integrated ac-dc SCOPF problem for real-world large-scale power systems such as the Australian NEM, ensuring AC feasible solutions. This methodology includes development of a SCOPF model based on a decomposition scheme that

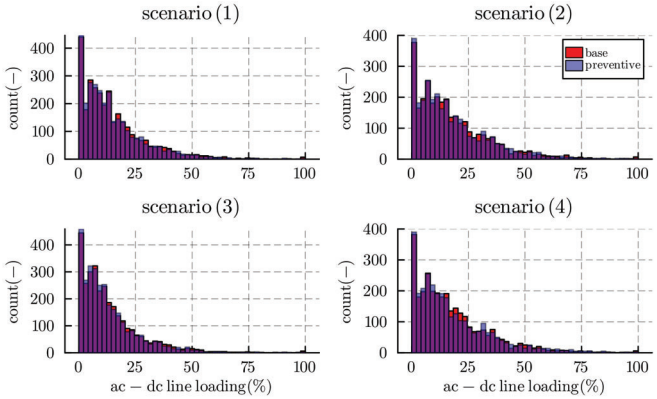

Fig. 5. Normalized ac-dc line loadings for base and preventive solutions using proposed SCOPF model.

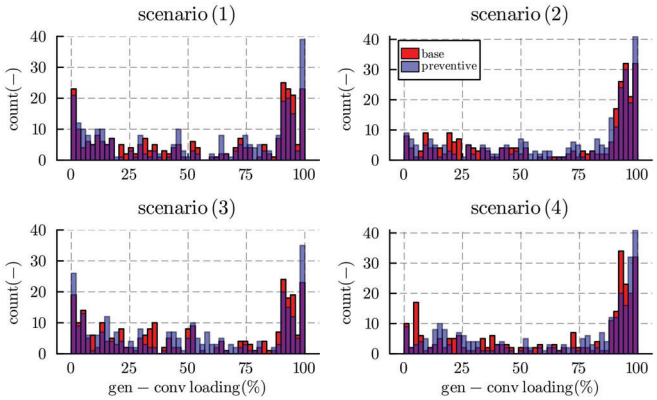

Fig. 6. Normalized generator and converter loadings for base and preventive solutions using proposed SCOPF model.

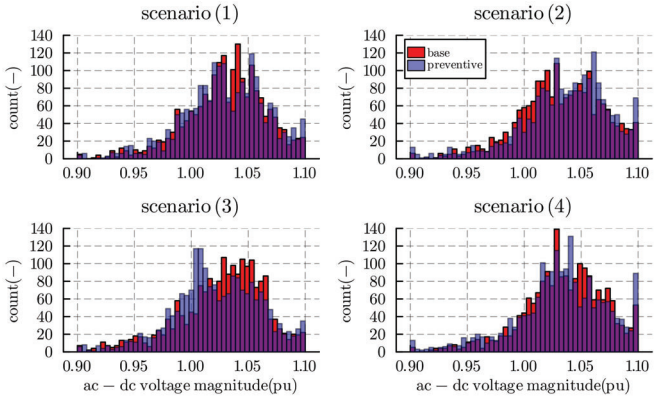

Fig. 7. ac-dc voltage magnitude for base and preventive solutions using proposed SCOPF model.

significantly reduced the dimensionality and thus improves the computation of the problem. Another important facet of this SCOPF model is the contingency ranking, evaluation, and non-dominated filtering algorithm, which further reduced the run-

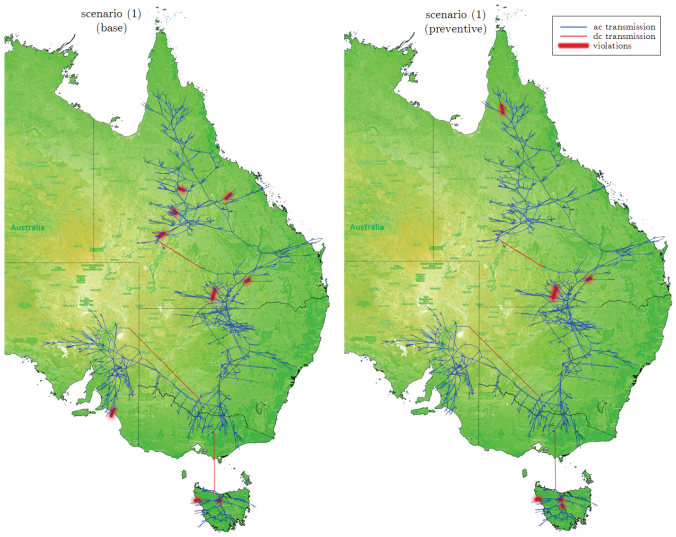

Fig. 8. ac-dc line violations at base and preventive solutions in scenario 1 using proposed SCOPF model.

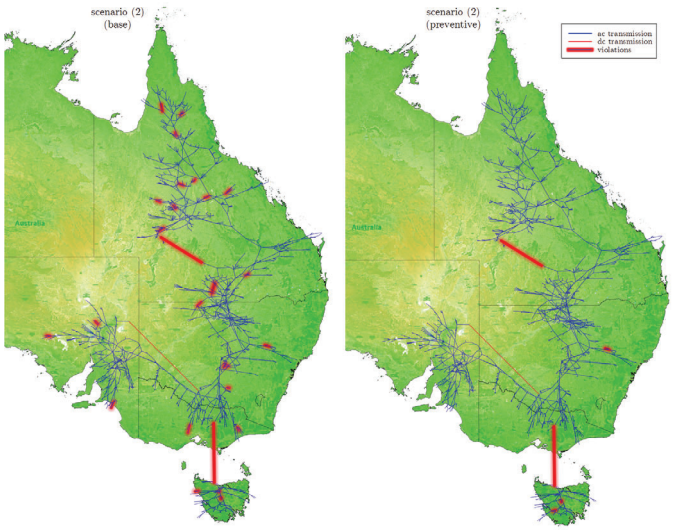

Fig. 9. ac-dc line violations at base and preventive solutions in scenario 2 using proposed SCOPF model.

time. Moreover, the cyclic selection of contingencies, careful choice of slack variables, and a tailored warm start also added to the performance as demonstrated in the case studies. This developed ac-dc SCOPF tool is made available as an open-source library 'PowerModelsACDCsecurityconstrained.jl'.

The proposed ac-dc SCOPF model is validated against the conventional TSMP model on four different test cases `case5`, `case24`, `case67`, `case500`, and the results indicate that with slightly higher operating costs same contingencies are secured but in far less time. The results show that the proposed model efficiently solves `S-NEM2000_acdc` to provide preventive solutions in less than 5 min resembling the NEM operating window with a large contingency set including

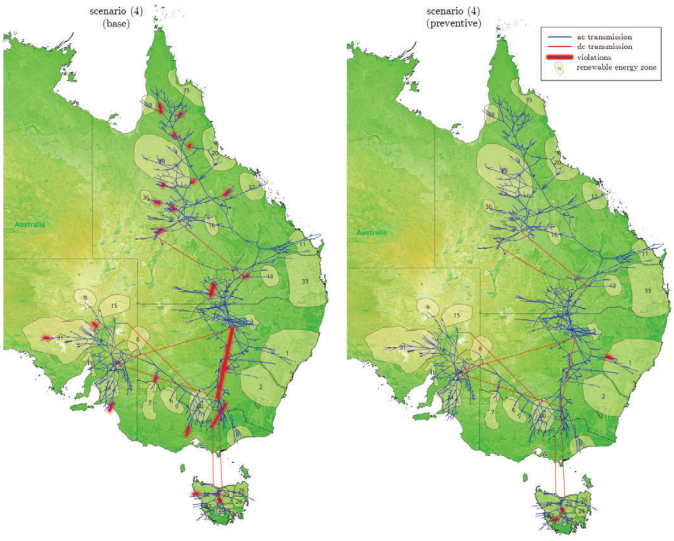

Fig. 10. ac-dc line violations at base and preventive solutions in scenario 4 using proposed SCOPF model.

ac branch (lines and transformers), HVDC converter, and generator contingencies under four different scenarios. The scenarios include high to minimum load variation, renewable energy zone integration, and additional reinforcements including point-to-point and meshed HVDC thus proving the efficacy of the model in real-time applications and planning studies.

Future work will involve accurate modeling of voltage constraints, generator and converter frequency and voltage droop characteristics, frequency reserves (FCAS), droop coefficients, and online participation factors to improve the accuracy of the obtained solutions.

References

[1] R. Heidari, M. Amos, and F. Geth, "An open optimal power flow model for the australian national electricity market," 2023.

[2] A. Blakers, M. Stocks, B. Lu, C. Cheng, and R. Stocks, "Pathway to 100% renewable electricity," *IEEE Journal of Photovoltaics*, vol. 9, no. 6, pp. 1828–1833, 2019.

[3] D. McConnell, S. Holmes à Court, S. Tan, and N. Cubrilovic, "An open platform for national electricity market data," 2022. [Online]. Available: https://opennem.org.au/energy/nem/?range=1y&interval=1w

[4] AEMC, "National electricity rules - power system security." [Online]. Available: https://energy-rules.aemc.gov.au/ner/384/104415

[5] Y. Pang, X. Qu, Z. Ren, and J. Mei, "A novel coordinated control strategy for lcc/vsc hybrid dc distribution power system," *EEE J. Emerg. Sel. Top. Circuits Syst.*, vol. 13, no. 2, pp. 629–636, 2023.

[6] M. Goodarzi and Q. Li, "Hybrid physics and data-driven contingency filtering for security operation of micro energy-water nexus," *CSEE J. Power Energy Syst.*, pp. 1–9, 2023.

[7] H. Ergun, J. Dave, D. Van Hertem, and F. Geth, "Optimal power flow for ac-dc grids: Formulation, convex relaxation, linear approximation, and implementation," *IEEE Trans. Power Syst.*, vol. 34, no. 4, pp. 2980–2990, 2019.

[8] K. Baker, "Solutions of dc opf are never ac feasible," ser. e-Energy. New York, NY, USA: ACM, 2021, p. 264–268.

[9] I.-I. Avramidis, F. Capitanescu, S. Karagiannopoulos, and E. Vrettos, "A novel approximation of security-constrained optimal power flow with incorporation of generator frequency and voltage control response," *IEEE Trans. Power Syst.*, vol. 36, no. 3, pp. 2438–2447, 2021.

[10] P. Sun, H. R. Wickramasinghe, M. Khalid, and G. Konstantinou, "Ac/dc fault handling and expanded dc power flow expression in hybrid multi-converter dc grids," *Int. J. Elec. Power Energy Syst.*, vol. 141, p. 107989, 2022.

[11] J. Cao, W. Du, and H. Wang, "An improved corrective security constrained OPF for meshed ac/dc grids with multi-terminal VSC-HVDC," *IEEE Trans. Power Syst.*, vol. 31, no. 1, pp. 485–495, 2015.

[12] J. Mohammadi, G. Hug, and S. Kar, "Agent-based distributed security constrained optimal power flow," *IEEE Trans. Smart Grid*, vol. 9, no. 2, pp. 1118–1130, 2016.

[13] M. Velay, M. Vinyals, Y. Besanger, and N. Retière, "Fully distributed security constrained optimal power flow with primary frequency control," *Int. J. Elect. Power & Energy Syst.*, vol. 110, pp. 536–547, 2019.

[14] A. Gholami, K. Sun, S. Zhang, and X. A. Sun, "An admm-based distributed optimization method for solving security-constrained ac optimal power flow," *arXiv preprint arXiv:2202.06787*, 2022.

[15] A. Velloso and P. Van Hentenryck, "Combining deep learning and optimization for preventive security-constrained dc optimal power flow," *IEEE Trans. Power Syst.*, vol. 36, no. 4, pp. 3618–3628, 2021.

[16] Z. Yan and Y. Xu, "A hybrid data-driven method for fast solution of security-constrained optimal power flow," *IEEE Trans. Power Syst.*, 2022.

[17] S. Liu, Y. Guo, W. Tang, H. Sun, W. Huang, and J. Hou, "Varying condition SCOPF optimization based on deep learning and knowledge graph," *IEEE Trans. Power Syst.*, 2022.

[18] A. Jacobson, F. Pecci, N. Sepulveda, Q. Xu, and J. Jenkins, "A computationally efficient benders decomposition for energy systems planning problems with detailed operations and time-coupling constraints," *arXiv preprint arXiv:2302.10037*, 2023.

[19] A. Velloso, P. Van Hentenryck, and E. S. Johnson, "An exact and scalable problem decomposition for security-constrained optimal power flow," *Elect. Power Syst. Res.*, vol. 195, p. 106677, 2021.

[20] M. Bazrafshan, K. Baker, and J. Mohammadi, "Computationally efficient solutions for large-scale security-constrained optimal power flow," 2020.

[21] R. Weinhold and R. Mieth, "Fast security-constrained optimal power flow through low-impact and redundancy screening," *IEEE Trans. Power Syst.*, vol. 35, no. 6, pp. 4574–4584, 2020.

[22] N. Popli, E. Davoodi, F. Capitanescu, and L. Wehenkel, "On the robustness of machine-learnt proxies for security constrained optimal power flow solvers," 2023.

[23] K. Meng, W. Zhang, Y. Li, Z. Y. Dong, Z. Xu, K. P. Wong, and Y. Zheng, "Hierarchical SCOPF considering wind energy integration through multiterminal vsc-hvdc grids," *IEEE Trans. Power Syst.*, vol. 32, no. 6, pp. 4211–4221, 2017.

[24] G. Mohy-ud din, R. Heidari, H. Ergun, and F. Geth, "An ac-dc power flow algorithm for australian national electricity market," in *2023 IEEE International Conference on Energy Technologies for Future Grids (ETFG)*, 2023, pp. 1–6.

[25] Q. Jiang and K. Xu, "A novel iterative contingency filtering approach to corrective security-constrained optimal power flow," *IEEE Trans. Power Syst.*, vol. 29, no. 3, pp. 1099–1109, 2014.

[26] Y. Li and Y. Li, "Security-constrained multi-objective optimal power flow for a hybrid ac/vsc-mtdc system with lasso-based contingency filtering," *IEEE Access*, vol. 8, pp. 6801–6811, 2019.

[27] F. Karbalaei and S. Abbasi, "L-index based contingency filtering for voltage stability constrained reactive power planning," *Turkish J. Elec. Eng. Comp. Sci.*, vol. 26, no. 6, pp. 3156–3167, 2018.

[28] F. Karbalaei, H. Shahbazi, and M. Mahdavi, "A new method for solving preventive security-constrained optimal power flow based on linear network compression," *Int. J. Elec. Power Energy Syst.*, vol. 96, pp. 23–29, 2018.

[29] F. E. Curtis, D. K. Molzahn, S. Tu, A. Wächter, E. Wei, and E. Wong, "A decomposition algorithm for large-scale security-constrained ac optimal power flow," 2021.

[30] K. den Bergh, E. Delarue, W. D'haeseleer *et al.*, "Dc power flow in unit commitment models," *KU Leuven Energy Institute*, 2014.

[31] A. Moreira, A. Valenzuela, and M. Heleno, "Solving market-based large-scale security-constrained ac optimal power flows," *IEEE Trans. on Power Syst.*, 2022.

[32] F. Capitanescu, M. Glavic, D. Ernst, and L. Wehenkel, "Contingency filtering techniques for preventive security-constrained optimal power flow," *IEEE Trans. Power Syst.*, vol. 22, no. 4, pp. 1690–1697, 2007.

[33] Mohy-ud-din, Ghulam and R. Heidari. [Online]. Available: https://github.com/csiro-energy-systems/PowerModelsACDCsecurityconstrained.jl